LINEAR COUPLED ATTITUDE-ORBIT CONTROL THROUGH AERODYNAMIC FORCES

Andrew Harris*, Christopher D. Petersen†, and Hanspeter Schaub‡

Spacecraft in Low Earth Orbit (LEO) typically consider atmospheric drag as a primary disturbance force. Growing interest in fuel-constrained small satellites, large LEO constellations, and robustness under thruster failure has motivated these drag forces for orbit control. The dependence of drag forces on a spacecraft's flow-wise projected area drives coupling between attitude and orbit states. A nonlinear model for attitude-driven drag based on collections of flat facets is presented and linearized about a reference orbit-attitude configuration, transforming the nonlinear orbit control problem into a linear differential-drag relative motion problem. The linearized dynamic model is used to provide insight into the controllability or lack thereof of relative orbit states from attitude alone given selected "deputy" and "chief" geometries/attitudes. Furthermore, the system's controllability is demonstrated under both linearized and nonlinear dynamics using a Linear Quadratic Regulator (LQR)-derived controller. While sensitive to the selection of state and control tuning parameters, this control strategy shows good convergence under the key assumptions of local relative motion and small attitude variation.

Nomenclature

$\boldsymbol{r}$	Vector
$\boldsymbol{r}_{O/H}$	Vector from point O to point H
r	Magnitude of vector $\boldsymbol{r}$
$[R]$	Denotes a matrix, R
$\hat{\boldsymbol{r}}$	Unit vector
$\tilde{\boldsymbol{r}}$	Skew-symmetric matrix of vector $\boldsymbol{r}$
${}^{\mathcal{B}}\boldsymbol{r}$	Vector expressed in B frame
$\dot{r}$	Inertial time derivative
${}^{\mathcal{B}}\frac{dr}{dt}$	Time derivative as seen by B frame
$[BN]$	Rotation matrix from frame N to frame B
C_D	Nondimensional drag coefficient
C_L	Nondimensional lift coefficient
$\boldsymbol{\omega}_{B/N}$	Spacecraft angular velocity vector between frames B and N
ρ	Local neutral atmospheric density
A	Area

Subscript

n	Panel normal vector
p	Panel position vector
i	Panel number

*Research Assistant, Ann and H.J. Smead Department of Aerospace Engineering Sciences, Graduate Student, University of Colorado Boulder, Boulder, CO, 80309 USA.

†Research Engineer, Air Force Research Laboratory Space Vehicles Directorate, Kirtland AFB, NM.

‡Alfred T. and Betty E. Look Professor of Engineering, Department of Aerospace Engineering Sciences, University of Colorado, 431 UCB, Colorado Center for Astrodynamics Research, Boulder, CO 80309-0431. AAS Fellow.

I. Introduction

Atmospheric forces on spacecraft have long been recognized as an avenue for coupling between attitude and orbital dynamics.[1] Owing to its dependence on atmospheric density, these forces and torques are small relative to gravity and are typically considered as perturbations in the context of orbital motion. However, at LEO altitudes, forces from atmospheric interactions can have substantial impacts on spacecraft orbits.[2] For spacecraft that lack the volume or mass to mount thrusters (such as cubesats) or those whose thrusters are disabled but which maintain attitude control through other means, the coupling between attitude and orbital motion through drag presents one method of recovering mission utility. Additionally, there is rising interest in large LEO constellations for telecommunication and Earth-imaging. In this context, drag-enabled attitude-orbit coupling could provide a propellant-free method for formation constitution and maintenance, thereby extending mission lifetimes and reducing constellation costs.

In concept, this work is similar to an existing body of literature that focuses on ballistic-coefficient controlled differential-drag formation flight. These techniques focus on the control of one or more spacecraft's ballistic coefficient by means of actuated flaps[3] or panels, and treat either the ballistic coefficient or the spacecraft flow-wise projected area as the primary control input.[4] The addition of actuated flaps and panels, while attractive for control purposes, unfortunately adds additional cost and system complexity that is undesirable for mission managers. Many spacecraft, including cubesats, have geometries whose projected areas vary with attitude as demonstrated in Figure 1.

Horsley et al[5] presents one method for incorporating the limitations of purely geometric-driven differential drag control as part of a two-step nonlinear planning and control routine. In this work, discrete attitude configurations are selected to produce positive, negative, and zero relative accelerations, effectively using the spacecraft attitude to provide "bang-bang" orbit control. This discrete-attitude-mode approach to differential drag flight is used operationally by Planet Labs for constellation constitution and maintenance on their large-scale Earth-imaging cubesat constellation.[6] This approach does not require complex, on-line modeling of spacecraft geometries and provides the maximum possible differential drag for a pair of spacecraft.

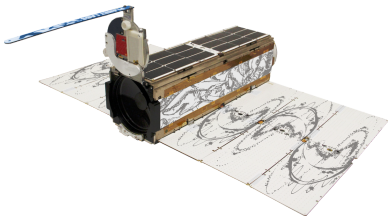

Figure 1: A PlanetLabs Dove spacecraft demonstrating non-uniform geometry

However, the "bang-bang" approach used by many discrete-attitude-mode controllers incurs substantial mission costs, due to both the time needed to conduct a maneuver and the potentially large attitude maneuvers needed to modulate the spacecraft attitude between configurations. For cubesats like the Planet Labs Dove, maneuvering between a minimum-drag and maximum-drag configuration requires a 90° slew. As such, spacecraft are not capable of conducting mission operations during orbit maintenance periods. Dell'Elce and Kerschen[7] present a method of single-axis attitude-driven orbit control for the QB50 constellation using an on-line optimizer and compensator. The computational intensiveness of this technique requires the use of approximations for online application, but nevertheless provides credibility to the concept of differential-drag control based on small attitude motions.

This work aims to improve the utility of drag-based orbital maneuvering by providing an alternative to bang-bang attitude-driven differential drag control. To do so, the coupling between spacecraft geometries and experienced drag through attitude must be explored directly. The influence of geometry and surface material properties on spacecraft drag is a subject of intense research due to its importance in both space object tracking and aeronomy studies. For analytic insight, facet-based models such as those explored by Sutton[8] provide reasonable accuracy and analytical insight into the dynamics of the "true" system. An alternative approach is the use of multi-particle Monte-Carlo (MPMC) or other MC-based methods to develop lookup tables or fitted analytical functions to approximate the real drag behavior of a given spacecraft. While potentially more accurate in the presence of concave geometries,[9] simple convex geometries are reasonably well-modeled by analytical expressions.

Coupling between translational and rotational motion has been treated extensively in the context of robotics, providing a beneficial framework for analyzing problems in astrodynamics. Filipe[10] develops a methodology for conducing coupled rotational-translational control for spacecraft rendezvous using a dual-quaternion representation of the attitude and orbit. Solar or electric sails, which also experience considerable attitude-orbit coupling, have served as the objects of study for coupled attitude-orbit control[11,12] . A common issue with these approaches is the lack of additional intuition gained through the use of compact translation-rotation representations such as dual quaternions. For these reasons, a straightforward linear model of the

underling relative dynamics is sought.

The paper is organized as follows. First, a nonlinear model of coupled attitude-orbit motion is presented in Section II.B. Next, this model is linearized about a selected reference orbit experiencing drag forces in Section II.D. Section II.E describes the linearization of the system's attitude dependence about a selected reference attitude producing a linear system. The linear controllability of this system is discussed in Section III.A. Finally, Section III.B describes the implementation and performance of a linear-quadratic regulator based on the linearized system on both the linearized and nonlinear dynamics.

II. Problem Statement

II.A. Frame Definitions

Before addressing the system dynamics, it is important to define the reference frames at play within the problem. First is the planet-centered inertial frame N whose center is the origin, which is written as:

$$N = \{\mathbf{0}, \hat{\boldsymbol{n}}_1, \hat{\boldsymbol{n}}_2, \hat{\boldsymbol{n}}_3\} \tag{1}$$

Next is the Hill frame H, which is centered on the spacecraft at a given position $\boldsymbol{r}_{H/N}$ in orbit and consists of the following unit vectors:

$$H = \{\boldsymbol{r}_{H/N}, \hat{\boldsymbol{h}}_r, \hat{\boldsymbol{h}}_\theta, \hat{\boldsymbol{h}}_3\} \tag{2}$$

where $\boldsymbol{r}_{H/N}$ is the position vector of the spacecraft with respect to the center of the N frame and the unit vectors are defined as follows:

$$\hat{\boldsymbol{h}}_r = \frac{\boldsymbol{r}_{H/N}}{\|\boldsymbol{r}_{H/N}\|} \tag{3}$$

$$\hat{\boldsymbol{h}}_3 = \frac{\boldsymbol{r}_{H/N} \times \dot{\boldsymbol{r}}_{H/N}}{\|\boldsymbol{r}_{H/N}\|\|\dot{\boldsymbol{r}}_{H/N}\|} \tag{4}$$

$$\hat{\boldsymbol{h}}_\theta = \hat{\boldsymbol{h}}_3 \times \hat{\boldsymbol{h}}_r \tag{5}$$

The matrix that maps from H to N, $[HN]$, is expressed by:

$$[HN] = \begin{bmatrix} \hat{\boldsymbol{h}}_r^T \\ \hat{\boldsymbol{h}}_\theta^T \\ \hat{\boldsymbol{h}}_3^T \end{bmatrix} \tag{6}$$

The angular velocity of H with respect to N is given by the spacecraft's mean motion n, which forms the angular velocity vector ${}^{\mathcal{N}}\boldsymbol{\omega}_{H/N} = \begin{bmatrix} 0 & 0 & \dot{f} \end{bmatrix}^T$, where $\dot{f}$ is the orbit true anomaly rate. For circular orbits, the true anomaly rate is equal to the mean anomaly rate n.

Finally, the body frame B is defined, which is aligned with the spacecraft's principal inertia frame and written as the following:

$$B = \{\boldsymbol{r}_{H/N}, \hat{\boldsymbol{b}}_1, \hat{\boldsymbol{b}}_2, \hat{\boldsymbol{b}}_3\} \tag{7}$$

The angular velocity vector between the body and inertial frames is given generally as:

$${}^{\mathcal{B}}\boldsymbol{\omega}_{B/N} = \begin{bmatrix} \omega_1 & \omega_2 & \omega_3 \end{bmatrix}^T \tag{8}$$

II.B. Nonlinear Dynamics

With the system reference frames established, it is possible to sensibly describe the dynamics that underly this work. A spacecraft experiencing spherical two-body gravity with other perturbation accelerations obeys the following equations of motion:[13]

$$\ddot{\boldsymbol{r}} = \frac{-\mu}{r^3}\boldsymbol{r} + \boldsymbol{a}_p \tag{9}$$

where $\mathbf{r}$ is the inertial spacecraft position vector, μ is the planet's gravitational parameter, and $\mathbf{a}_p$ is the inertial perturbing acceleration vector. In this work, the perturbing accelerations are considered to be due only to attitude-dependent drag. For analyses in LEO, the intended regime, this assumption is reasonable.[13]

The drag acting on a given spacecraft is assumed to follow the commonly-used quadratic expression for drag:[13]

$$\boldsymbol{a}_p = -\frac{1}{2}\beta_d P(\boldsymbol{v}^T\boldsymbol{v})\hat{\boldsymbol{v}} \tag{10}$$

in which β_D represents the spacecraft ballistic coefficient, P is used to represent the local atmospheric density, $\boldsymbol{v}$ is the flow-relative velocity of the spacecraft, and $\hat{\boldsymbol{v}}$ is the unit direction of the flow-relative velocity.

Attitude dependence is considered to enter into the system primarily through the dependence of the ballistic coefficient β_D on projected area. Considering a spacecraft consisting of several flat faceted panels with individual areas A_i, individual drag coefficients $C_{D,i}$, and individual orientations in the body frame $\hat{n}_i$, the drag acceleration due to a single panel can be written using this expression suggested by Sutton:[8]

$${}^{\mathcal{N}}\boldsymbol{a}_{D,i} = -\frac{1}{2m_i}C_{D,i}A_i({}^{\mathcal{B}}\hat{\boldsymbol{n}}_i \cdot [BN]^{\mathcal{N}}\hat{\boldsymbol{v}})P(\boldsymbol{v}^T\boldsymbol{v})^{\mathcal{N}}\hat{\boldsymbol{v}} \tag{11}$$

Equation 11 is related to Equation 10 by:

$$\beta_{d,i} = \frac{C_{D,i}A_i({}^{\mathcal{B}}\hat{\boldsymbol{n}}_i \cdot [BN]^{\mathcal{N}}\hat{\boldsymbol{v}})}{m_i} \tag{12}$$

where m_i is the spacecraft mass.

Here, the dependence of $C_{D,i}$ on the plate attitude not considered in this analysis. Sutton[8] presents a gas-surface interaction model to define the dependence of the drag coefficient on flow geometry and plate material properties. These effects are typically only significant at oblate particle-surface interaction geometries and for spacecraft with small surface accomodation coefficients; as the expected value for surface accomodation coefficients has been empirically observed to be near 1, these effects are considered negligible for the purposes of this work.

II.C. Nonlinear Relative Dynamics

For orbits in LEO, drag forces alone achieve limited controllability with respect to orbits. In general, they can only be used to reach orbits with equal inclinations (as drag is an in-plane force) and lower energies. Instead of considering the case of general LEO orbits, the problem scope is restricted to consider only the relative motion between spacecraft experiencing atmospheric drag forces.

Classic relative motion equations describe the motion of a "deputy" spacecraft as seen by a "chief" spacecraft. The positions of these two spacecraft are related by the following expression:

$$\boldsymbol{r}_d = \boldsymbol{r}_c + \boldsymbol{\rho} \tag{13}$$

in which $\boldsymbol{\rho}$ is introduced to represent the relative position between the chief and deputy. Taking two inertial derivatives results in the following relationship between the accelerations:

$$\ddot{\boldsymbol{r}}_d = \ddot{\boldsymbol{r}}_c + \ddot{\boldsymbol{\rho}} \tag{14}$$

From this, we can solve for the relative acceleration vector and substitute in the chief and deputy accelerations given by Equation 9:

$$\ddot{\boldsymbol{\rho}} = \ddot{\boldsymbol{r}}_d - \ddot{\boldsymbol{r}}_c \tag{15}$$

$$\ddot{\boldsymbol{\rho}} = \frac{-\mu}{r_d^3}\mathbf{r_d} + \mathbf{a}_{D,d} - \frac{-\mu}{r_c^3}\mathbf{r_c} - \mathbf{a}_{D,c} \tag{16}$$

in which $\mathbf{a}_{D,c}$ and $\mathbf{a}_{D,d}$ are used to represent the drag accelerations of the chief and deputy, respectively. Substituting in Equation 13 results in:

$$\ddot{\boldsymbol{\rho}} = \frac{-\mu}{(r_c+\rho)^3}(\boldsymbol{r}_c + \boldsymbol{\rho}) + \frac{\mu}{r_c^3}\mathbf{r_c} + \mathbf{a}_{D,d} - \mathbf{a}_{D,c} \tag{17}$$

II.D. Linear Relative Dynamics with Drag

The nonlinear dynamics expressed in Equation 17 provide little a-priori analytical insight into the behavior of relative spacecraft motion under drag. To this end, Silva[14] provides one set of analytical expressions for relative motion under the assumption of atmospheric drag, small relative positions and velocities, and circular chief orbits, effectively constituting a "Hill-Clohessy-Whitshire plus drag" formulation for differential drag motion. Rotated into the aforementioned Hill frame and taking $\boldsymbol{\rho} = \begin{bmatrix} x & y & z \end{bmatrix}^T$, these equations are:

$$\ddot{x} = 2\dot{y}n + 3n^2x - \frac{1}{2}\beta_d P_d n r_c \dot{x} \tag{18}$$

$$\ddot{y} = -2\dot{x}n - n^2 r_c^2 \frac{1}{2}(\beta_C P_C - \beta_d P_d) - \beta_d P_d n r_c \dot{y} \tag{19}$$

$$\ddot{z} = -zn^2 - \frac{1}{2}(\beta_d P_d r_c n)\dot{z} \tag{20}$$

We note several changes relative to the classical HCW equations:

1. A secular drift term now exists in the y direction, proportional to the difference in ballistic coefficient between the chief and deputy
2. Relative-velocity-proportional drag terms now exist in every axis, including the z axis.
3. Chief-driven drag terms exist only in the y-(velocity) axis.

For static relative equilibria to exist, both the first and second order derivatives must be zero. Setting the second order derivatives equal to zero yields the following expressions:

$$\frac{1}{2}\beta_d P_d r_c \dot{x} = 2\dot{y} + 3nx \tag{21}$$

$$n^2 r_c^2 \frac{1}{2}(\beta_C P_C - \beta_d P_d) + \beta_d P_d n r_c \dot{y} = -2\dot{x}n \tag{22}$$

$$\frac{1}{2}(\beta_d P_d r_c n)\dot{z} = -zn^2 \tag{23}$$

Immediately, it is apparent that a secular drift term exists in the y direction due to the differential drag force acting between the deputy and chief, without a dependence on the relative velocity. Additionally zeroing the first-order derivatives yields:

$$0 = 3nx \tag{24}$$

$$n^2 r_c^2 \frac{1}{2}(\beta_C P_C - \beta_d P_d) = 0 \tag{25}$$

$$0 = -zn^2 \tag{26}$$

which suggests that the system origin is a static equilibrium when the differential drag term $n^2 r_c^2 \frac{1}{2}(\beta_C P_C - \beta_d P_d)$ is zeroed.

As such, in addition to the classic HCW conditions for static equilibria, it is additionally necessary to ensure that the deputy and chief values of the ballistic coefficient and local neutral density match. This is an important consideration for control purposes, as it defines a condition for unforced equilibrium in the attitude-driven system.

For the case in which P_C and P_D match—i.e., when the position of the chief and deputy are close—it is necessary for the ballistic coefficients of the chief and deputy to match to avoid secular drift in the y direction.

II.E. Attitude Dependence

Linear equations of motion including assumed control forces enable the application of convenient and intuitive linear controls tools; as such it is desirable to re-write the attitude-dependent drag expression given by Equation 11 in terms of variations from a nominal attitude. To do so, an additional "Target" frame T is defined with a corresponding attitude matrix $[TB]$. To improve the linearization's validity, Modified Rodriguez Parameters (MRPs) are selected as the attitude parametrization for this linearization:

$$A_p = A_i(\hat{\boldsymbol{n}}^T[TB(\boldsymbol{\sigma}_p)][BN(\boldsymbol{\sigma}_r)]^{\mathcal{N}}\hat{\boldsymbol{v}}) \tag{27}$$

Without loss of generality, the inertial velocity direction is also rotated into the chief Hill reference frame. Under the assumption of circular orbits, the inertial direction of the velocity vector in the chief reference frame is simply parallel to the $\hat{\boldsymbol{h}}_\theta$ unit vector. Under these assumptions, the facet projected area becomes:

$$A_p = A_i(\hat{\boldsymbol{n}}^T[TB(\boldsymbol{\sigma}_p)][BH(\boldsymbol{\sigma}_r)]^{\mathcal{H}}\hat{\boldsymbol{v}}) \tag{28}$$

Assuming that σ_p is small such that second order terms can be neglected, $[TB(\boldsymbol{\sigma}_p)]$ is written as:

$$A_p = A_i(\hat{\boldsymbol{n}}^T[BN(\boldsymbol{\sigma}_r)]\hat{\boldsymbol{v}} - 4\hat{\boldsymbol{n}}^T[\tilde{\boldsymbol{\sigma}}_p][BN(\boldsymbol{\sigma}_r)]\hat{\boldsymbol{v}}) \tag{29}$$

This expression contains two primary components: a constant term driven by the selected reference MRP, and a linearized rotational component based on the perturbing MRP.

II.F. State-Space Representation

The existence of linear approximations for both the system dynamics and the assumed control input lend themselves to the use of linear controllability tools. These tools provide an intuitive framework to examine the properties of this coupled, pseudo-linear system. This class of analysis requires a system of the following form:

$$\dot{\boldsymbol{x}} = [A]\boldsymbol{x} + [B]\boldsymbol{u} \tag{30}$$

Unfortunately, the second-order relative equations of motion given in Equations 18-20 contain secular drift terms proportional to the deputy-chief differential drag ($\beta_C P_C - \beta_D P_D$). Under the assumption of similar deputy and chief geometries, this term can be reasonably assumed to go to zero, as $\beta_C = \beta_D$ for identical reference geometries and attitudes, and $P_D = P_C$ as $\boldsymbol{\rho}$ goes to $\mathbf{0}$. This assumption is reasonable for formation-keeping in a constellation, or in the case of a fictitious "reference" chief.

To form the control effects matrix B, the partials of Equations 21-23 are taken with respect to the small control attitude σ_p. Noting that only the deputy ballistic coefficient is dependent on σ_p, partials are taken as follows:

$$\frac{\delta\beta_d}{\delta\boldsymbol{\sigma}_p} = -4\frac{C_{D,d}}{m}A_i\hat{\boldsymbol{n}}^T\frac{\delta}{\delta\sigma_p}([\tilde{\boldsymbol{\sigma}}_p][BN(\boldsymbol{\sigma}_r)]\hat{\boldsymbol{v}}) \tag{31}$$

Here, the properties of the cross product matrix are exploited to make the derivative more obvious. For arbitrary vectors $\boldsymbol{a}$ and $\boldsymbol{b}$ and for an arbitrary matrix $[Z]$, the following properties hold:

$$[\tilde{\boldsymbol{a}}]\boldsymbol{b} = -[\tilde{\boldsymbol{b}}]a \tag{32}$$

$$\frac{\delta}{\delta\boldsymbol{x}}[Z]\boldsymbol{x} = [Z] \tag{33}$$

To simplify the notation, the intermediate vector $\hat{\boldsymbol{q}} = [[BN(\boldsymbol{\sigma}_r)]\hat{\boldsymbol{v}}$ is introduced. Applying these properties to the derivatives in Equation 31 yields:

$$\frac{\delta\beta_d}{\delta\boldsymbol{\sigma}_p} = 4\frac{C_{D,d}}{m}A_i\hat{\boldsymbol{n}}^T([\tilde{\hat{\boldsymbol{q}}}]) \tag{34}$$

By inspection, this derivative forms a 1×3 row vector. This is as expected for the rows of $[B]$. Applying this definition to the linear equations of motion assuming nominal known initial conditions results in the

following partials:

$$\frac{\delta \ddot{x}}{\delta \boldsymbol{\sigma}_p} = -\frac{1}{2} P_d n r_c \dot{x}_0 \frac{\delta \beta_d}{\delta \boldsymbol{\sigma}_p} \tag{35}$$

$$\frac{\delta \ddot{y}}{\delta \boldsymbol{\sigma}_p} = (\frac{1}{2} n^2 r_c^2 P_d - P_d n r_c \dot{y}_0) \frac{\delta \beta_d}{\delta \boldsymbol{\sigma}_p} \tag{36}$$

$$\frac{\delta \ddot{z}}{\delta \boldsymbol{\sigma}_p} = -\frac{1}{2} (P_d r_c n) \dot{z}_0 \frac{\delta \beta_d}{\delta \boldsymbol{\sigma}_p} \tag{37}$$

An unfortunate consequence of this linearizion is that the relative acceleration partials are dependent upon the selection of initial or selected reference relative velocities. From these equations, the B matrix is written as:

$$[B] = \begin{bmatrix} \mathbf{0}_{3\times 3} \\ -\frac{1}{2} P_d n r_c \dot{x}_0 \frac{\delta \beta_d}{\delta \boldsymbol{\sigma}_p} \\ (\frac{1}{2} n^2 r_c^2 P_d - P_d n r_c \dot{y}_0) \frac{\delta \beta_d}{\delta \boldsymbol{\sigma}_p} \\ -\frac{1}{2} (P_d r_c n) \dot{z}_0 \frac{\delta \beta_d}{\delta \boldsymbol{\sigma}_p} \end{bmatrix}, \ \boldsymbol{u} = \begin{bmatrix} \sigma_{p,1} \\ \sigma_{p,2} \\ \sigma_{p,3} \end{bmatrix} \tag{38}$$

III. Controllability Analysis and Controller Implementation

III.A. Controllability Analysis

Equations 18-20 and Equation 35-37 define a linear set of equations of motion for a deputy-chief pair with the deputy attitude as an input. While these equations of motion are general with regards to deputy and chief geometry, a restricted case dealing with identical deputy/chief geometries is used to demonstrate the controllability properties of this system. This can be considered to represent multiple use cases. One example is maneuvering to a predefined reference orbit and attitude during formation constitution (i.e., rendezvous with a fictional chief). For rendezvous with a fictitious chief, it is desirable for the fictional chief orbit to have identical drag parameters to the real deputy. Alternatively, one could consider a rendezvous between identical spacecraft performing on-orbit assembly. In any of these cases, the system aim is to drive both the relative position and relative velocity states to zero.

The linearized equations derived in Section II.F enables the use of straightforward linear analysis tools to demonstrate controllability. A classic approach to understanding controllability for linear systems uses the controllability matrix, $[O]$, which is formed as:[15]

$$[O] = \begin{bmatrix} [B] & [A][B] & [A]^2[B] & \dots & [A]^{n-1}[B] \end{bmatrix} \tag{39}$$

where n is the number of system states, which for this system is six. The column and null spaces of $[O]$ form bases for the controllable and non-controllable subspaces for the system, respectively.

Due to the symbolic complexity of these expressions, a numerical example is provided to demonstrate the controllability properties of the linearized system. A reference system consisting of a single flat plate with dimensions, drag coefficient, and mass based upon those of a 3U cubesat with a three-meter by three-meter drag sail were used to numerically evaluate A and B for the purposes of forming O. The specific values used for these properties are listed in Table 1. Orbital elements for both the chief and deputy are given in Table 3. The matrix rank and QR factorization were computed using Numpy's `linalg` library.[16]

Table 1: : Spacecraft geometric parameters used for numerical controllability analysis.

Parameter	Chief Value	Deputy Value
P_i	2.7346*10^{-14} $\frac{\text{kg}}{\text{m}^3}$	2.7346*10^{-14} $\frac{\text{kg}}{\text{m}^3}$
A_i	9 m^2	9 m^2
m_i	3 kg	3 kg
$\hat{\boldsymbol{n}}_i$	$\begin{bmatrix} 0 & 1 & 0 \end{bmatrix}^T$	$\begin{bmatrix} 0 & 1 & 0 \end{bmatrix}^T$
$C_{d,i}$	2.2	2.2
σ_r	$\begin{bmatrix} 0 & 0 & 0.1989 \end{bmatrix}^T$	$\begin{bmatrix} 0 & 0 & 0.1989 \end{bmatrix}^T$

Three cases are examined: one in which the reference attitude is zero, representing a facet face-on into the flow; one in which the reference attitude is 0.5, representing a facet edge-on into the flow; and one in which the reference attitude is equivalent to a 45° rotation about the HCW $\hat{h}_3$ axis, representing an intermediate drag configuration.

This analysis reveals multiple phenomenon relating to the system's controllability. First, the selected reference attitude can restore or prevent controllability. This is sensible when considering the nature of the small-attitude assumption as it relates to the area projection term. This dependence is more explicit when considering the area projection in terms of a single principle attitude angle θ, in which case the projection can be rewritten as:

$$\hat{\boldsymbol{n}}^T \hat{\boldsymbol{v}} = \cos(\theta) \tag{40}$$

Linearizing the cosine term about a reference angle θ_r and considering a small perturbation angle, θ_p, yields:

$$\hat{\boldsymbol{n}}^T \hat{\boldsymbol{v}} = \cos(\theta_r + \theta_p) \tag{41}$$

If $\theta_r = 0$, corresponding to the face-on case, the effect of the perturbation angle drops out, explaining the loss of linear controllability. However, the edge-on case also presents an issue. For a physical plate, rotation in either direction represents an increase in the projected area. If the chief is assumed to be uncooperative, this means that the effective control input can never produce a negative acceleration, and as such a linear model cannot effectively approximate its behavior. This is illustrated in Figure 2, which demonstrates the variation of a single-plate deputy drag coefficient with attitude for reference attitude configurations facing into the flow, banked into the flow, and edge-on into the flow, and respectively. It is only in the banked case that control authority is provided about the described equilibrium condition in which the deputy and chief ballistic coefficients are equal.

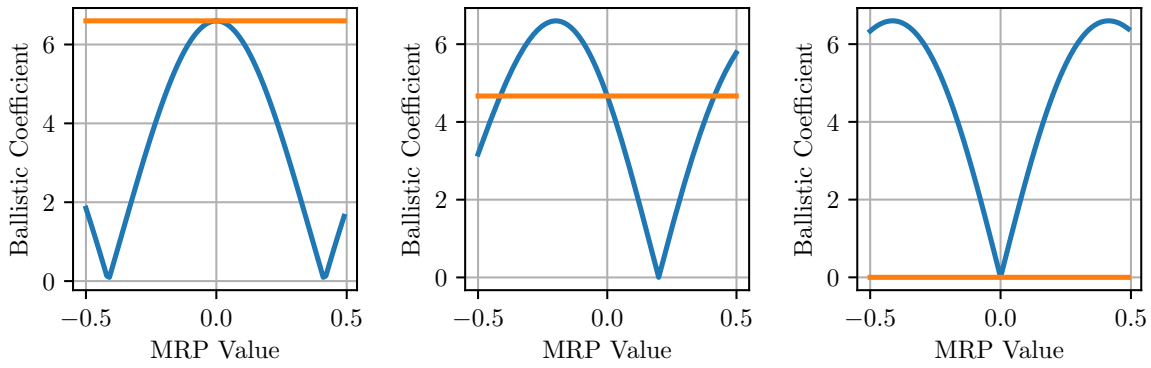

(a) Face-On Case (b) Banked Case (c) Edge-On Case

Figure 2: Deputy (Blue) and Chief (Orange) ballistic coefficients using reference numbers from Table 1. Results shown for face-on, banked, and edge-on reference attitudes.

This analysis provides a framework to understand admissible conditions and geometries for differential drag control inside and outside the linear regime. Differential drag formation flight requires that the deputy-chief pair be able to achieve both positive and negative relative accelerations from drag. In the attitude-only non-cooperative rendezvous case considered here, this requires that the deputy geometry and attitude allow it to both increase and decrease its drag profile relative to the chief.

Using the intermediate case angle as the reference angle, this analysis reveals that the in-plane states and velocities are controllable from attitude-driven drag alone. This aligns with our a-priori understanding of differential drag control and first-order relative motion. It is well-understood that the in-plane relative states are coupled, leading to the classic no-drift condition for linearized Cartesian relative motion and the widely-described "2 by 1 ellipse." Drag as a force is defined in opposition to a spacecraft's velocity direction, which is aligned with the $\hat{\boldsymbol{h}}_\theta$ axis for circular Chief orbits. From this, it is reasonable to conclude that in-plane states are controllable from relative velocity control alone. These results provide confidence in our model and approach, as they agree with results found in the literature for this class of control.[3]

III.B. Linear Control Implementation

Per the previous section, a subspace of the linearized system has been demonstrated to be linearly controllable. To this end, a straightforward linear control law based on LQR was developed and implemented for the sample linear system based on Table 1. Results are provided for two selected control objective weights — one which emphasized fast state performance (Case B), and one which emphasized economical use of the control input (Case A). Both the state gains $[Q]$ and the control gains $[R]$ are selected to be diagonal with elements of the magnitude stated in Table 2. The latter can be analogously considered as minimizing the variance from the desired reference attitude. For demonstration purposes, the control objective is to drive the deputy spacecraft to the chief position and velocity.

Table 2: : Selected control gains for Case A and Case B.

Control Design Variable	Case A Values	Case B Values
Q	1	0.1
R	1e4	1e7
dt	$5s$	$5s$

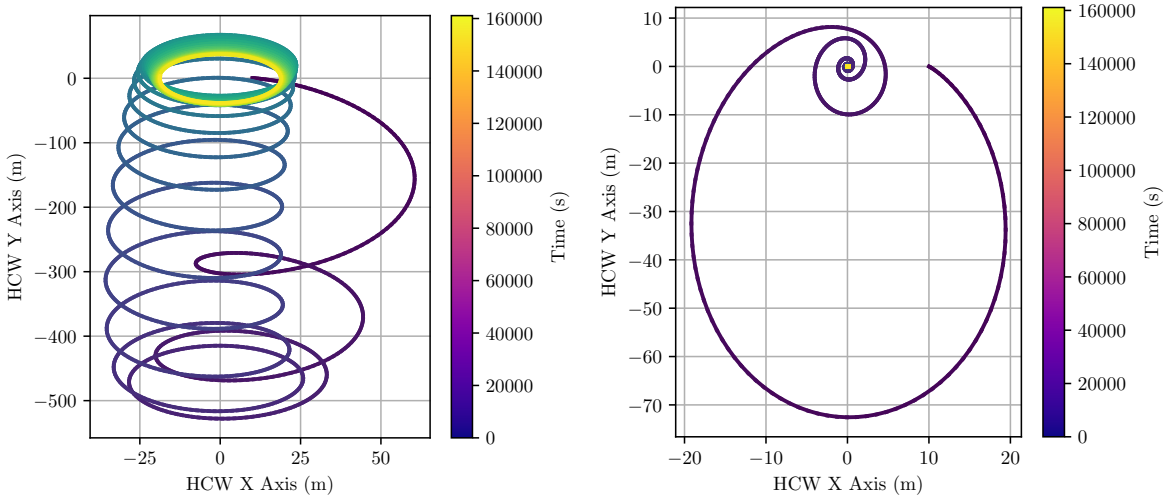

(a) Case A

(b) Case B

Figure 3: HCW x and y state evolution under linear dynamics with LQR-derived controller.

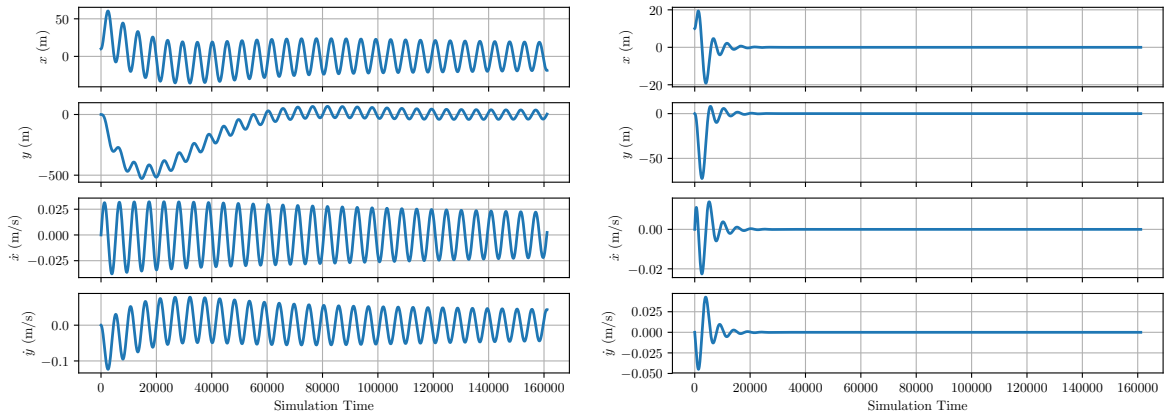

(a) Case A (b) Case B

Figure 4: Deputy relative position and velocity state trajectories in the chief Hill frame under attitude-driven control

With respect to the linearized system, both controls are found to be stabilizing, resulting in the state trajectories found in Figures 3 and 4. The commanded attitude MRPs are displayed in Figure 5. Notably, the commanded attitudes in the fast-state case vary far outside the domain in which MRP switching would typically be utilized ($\sigma^2 = 1$), suggesting that the system violates the small angle assumption critical to the linearization. Additionally, it is noted that the fast-state case displays substantial oscillation even after notionally reaching the reference states, though it is apparent from Figure 3a that its behavior is convergent towards the origin.

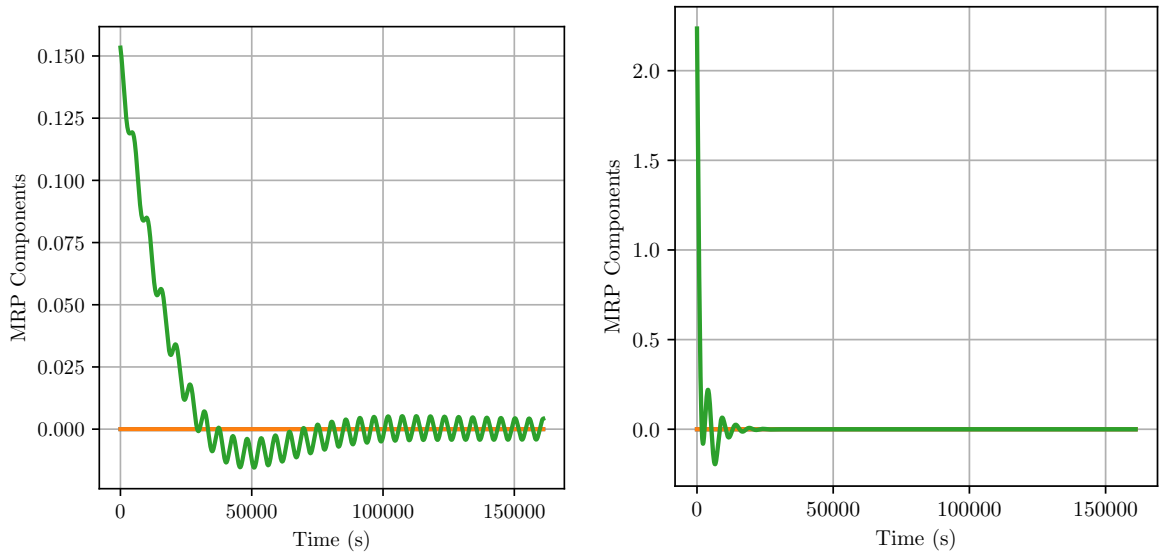

(a) Case A (b) Case B

Figure 5: Flow-relative attitude MRP component generated by the LQR-derived controller using linear dynamics under different control weights. Because the panel is rotated about one axis, only one MRP component is used for control.

To provide further validation of this approach, the linear controller was implemented on a system following the full nonlinear equations of motion found in Equation 16 under the same initial conditions and parameters used to generate the linearized system (i.e, those found in Tables 1-3). The selected scenario represents a slot-hoping maneuver, in which a spacecraft maneuvers to a selected reference location and attitude ahead of its current position on orbit. A small inclination difference is included to demonstrate the control's lack of

influence on out-of-plane motion as expected. The results of these simulations under both control strategies can be found in Figures 6-7. Attitude trajectories for these cases are shown in Figure 8.

Table 3: : Orbital elements for both the deputy and chief spacecraft.

Orbital Element	Chief Value	Deputy Value
a	250km + r_E	250km + r_E
i	45°	45.01°
e	0	0
Ω	20.0°	20.0°
ω	30.0°	30.0 °
M_0	20.0°	19.99°

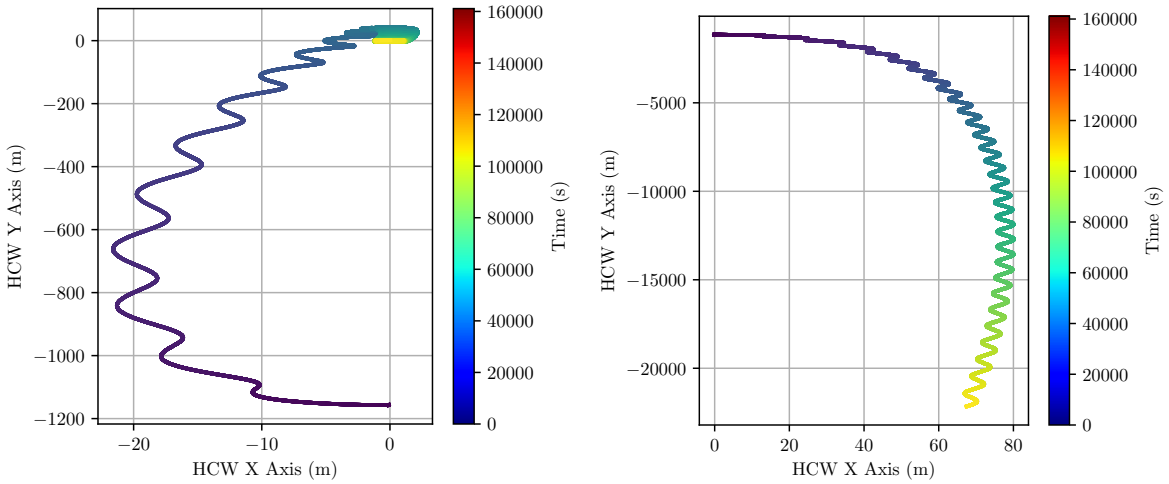

(a) Case A (b) Case B

Figure 6: HCW x and y state evolution under the LQR-derived controller on the assumed nonlinear system

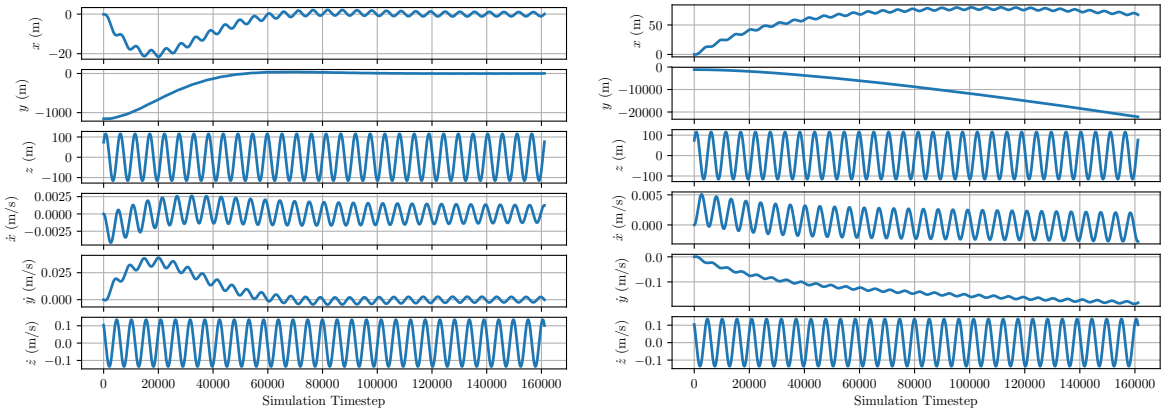

(a) Case A (b) Case B

Figure 7: Deputy relative position and velocity state trajectories in the chief Hill frame under attitude-driven control

Notably, the LQR controller derived for the linear system provides similar performance for the nonlinear system using Case A's control gains. This both validates the linearizations used to derive the LQR controller and demonstrates the applicability of the linearized system to the "real" problem at hand. However, the

results of Case B, which display state divergence from the reference, demonstrate limitations of the linearization approach. In Case B, the relatively large elements of $[B]$ cause the controller to request large attitudes outside the linear regime, a behavior shown in the linear system through Figure 5b.

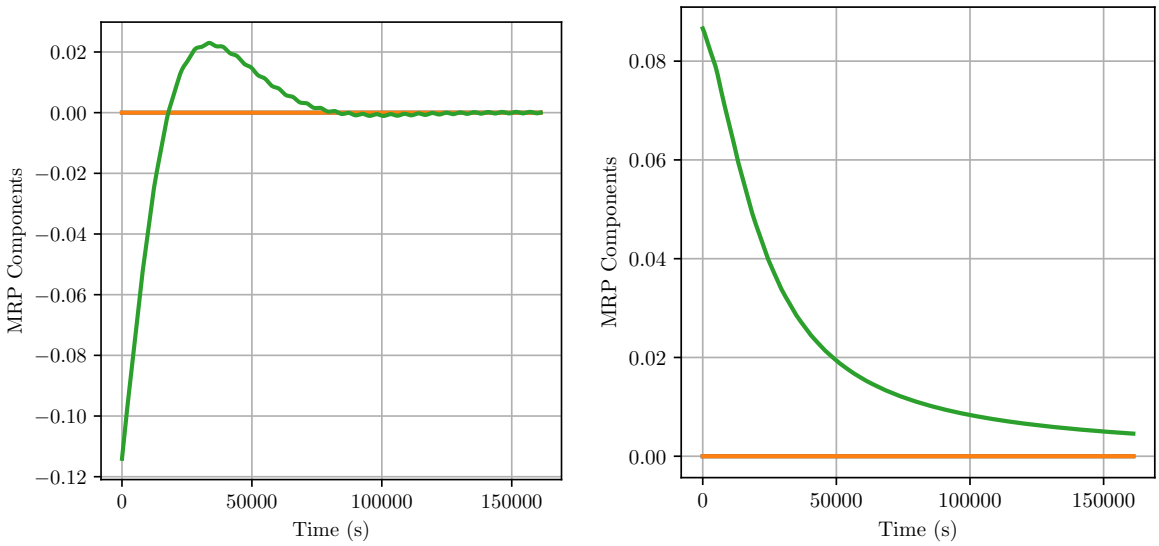

(a) Case A (b) Case B

Figure 8: Flow-relative attitude MRP component generated by the LQR-derived controller. Requested MRPs are transformed to the unit set.

These results demonstrate the need for "stiff" control gains in the linearized attitude-driven case. Nonlinearities present in the assumed input – the spacecraft's attitude – are the dominant driver of non-convergence for the controlled system.

IV. Conclusions and Future Work

Approaching drag-based orbital maneuvering as a two-step orbit formation and differential-drag rendezvous problem offers one answer to the problem of drag-based maneuvering in LEO, as it allows the transformation of a highly nonlinear orbit control problem into a simple linear differential-drag rendezvous problem. While considering single-plate deputy and chief geometries, the identification of admissible conditions for linear controllability and equilibrium can be readily extended to spacecraft consisting of many facets. This facet-driven controllability analysis allows multiple attitude configurations to be stitched together to provide a description of controllability in any given attitude configuration. This approach additionally allows the analysis of differential-drag rendezvous for spacecraft with different geometries, as would be used for non-cooperative rendezvous.

The validity of this linear controllability analysis is further demonstrated by the numerical simulations of Section III.B, which show the convergence of a linear control scheme for both the linearized and "true" nonlinear systems. These simulations also reveal a practical issue with the linearization of nonlinear attitude-geometry dynamics into a linear control input. This is manifested in the controller design through the weighting of state-convergence performance versus control economy, i.e. the relative sizes of $[Q]$ and $[R]$. Selection of large values of $[R]$ drives the controller to stay within the constraints of the attitude linearization. In practice, this could be accomplished by bounding the control input or using a "saturating" control law as opposed to the simple LQR-based controller used here.

Several potential opportunities for future work arise from this analysis. Firstly, the models of atmospheric drag could be extended to include attitude-based lift and drag coefficients discussed by Sutton et al. This would not only improve the fidelity of the linearization, but also allow it to be extended to differential-lift rendezvous, reducing the restriction of atmospheric maneuvering to in-plane positions.

Additionally, the described linear control routine is limited to situations fulfilling the admissible condi-

tions described in Section III.A, limiting its utility for general scenarios. Nonlinear stability and control approaches, such as Lyapunov-based techniques, have been used successfully in other differential-drag studies[17],[3] and present a promising avenue for working around the nonlinearities inherent to attitude dynamics.

V. Acknowledgements

This work was supported by the Department of Defense National Defense Science and Engineering Graduate Fellowship (NDSEG) Program, the Air Force Scholars Program, and the CU Smead Scholars Program.

References

[1]Schaub, H. and Junkins, J. L., *Analytical Mechanics of Space Systems*, American Institute of Aeronautics and Astronautics, 3rd ed., 2014.

[2]Marcos, F., Bowman, B., and Sheehan, R., "Accuracy of Earth's Thermospheric Neutral Density Models," *AIAA/AAS Astrodynamics Specialist Conference and Exhibit*, 2006, pp. 1–20.

[3]Pérez, D. and Bevilacqua, R., "Differential drag spacecraft rendezvous using an Adaptive Lyapunov Control strategy," *Advances in the Astronautical Sciences*, Vol. 145, 2012, pp. 973–991.

[4]Kumar, B. S., Ng, A., Yoshihara, K., and De Ruiter, A., "Differential drag as a means of spacecraft formation control," *IEEE Transactions on Aerospace and Electronic Systems*, Vol. 47, No. 2, 2011, pp. 1125–1135.

[5]Horsley, M., Nikolaev, S., and Pertica, A., "Small Satellite Rendezvous Using Differential Lift and Drag," *Journal of Guidance, Control, and Dynamics*, Vol. 36, No. 2, 2013, pp. 445–453.

[6]Foster, C., Hallam, H., and Mason, J., "Orbit determination and differential-drag control of Planet Labs cubesat constellations," *Advances in the Astronautical Sciences*, Vol. 156, 2016, pp. 645–657.

[7]Dellelce, L. and Kerschen, G., "Optimal propellantless rendez-vous using differential drag," *Acta Astronautica*, Vol. 109, 2015, pp. 112–123.

[8]Sutton, E., "Effects of Solar Disturbances on the Thermosphere Densities and Winds from CHAMP and GRACE Satellite Accelerometer Data," 2008, pp. 149.

[9]Pilinski, M. D., "Dynamic Gas-Surface Interaction Modeling for Satellite Aerodynamic Computations," 2011.

[10]Filipe, N. and Tsiotras, P., "Adaptive position and attitude tracking controller for satellite proximity operations using dual quaternions," *Advances in the Astronautical Sciences*, Vol. 150, 2014, pp. 2313–2332.

[11]Huo, M., Zhao, J., Xie, S., and Qi, N., "Coupled attitude-orbit dynamics and control for an electric sail in a heliocentric transfer mission," *PLoS ONE*, Vol. 10, No. 5, 2015, pp. 1–14.

[12]Mu, J., Gong, S., and Li, J., "Coupled Control of Reflectivity Modulated Solar Sail for GeoSail Formation Flying," *Journal of Guidance, Control, and Dynamics*, Vol. 38, No. 4, 2015, pp. 740–751.

[13]Vallado, D. A., *Fundamentals of Astrodynamcs and Applications*, Space Technology Library, 4th ed., 2013.

[14]Silva, E. D., "A Formulation of the Clohessy-Wiltshire Equations to Include Dynamic Atmospheric Drag," *AIAA/AAS Astrodynamics Specialist Conference*, , No. August, 2008.

[15]Brogan, W. L., *Modern Control Theory*, Prentice-Hall Inc, Englewood Cliffs, New Jersey, 3rd ed., 1991.

[16]Jones, E., Oliphant, T., Peterson, P., et al., "SciPy: Open source scientific tools for Python," 2001–, [Online; accessed 12/1/2017].

[17]Ben-Yaacov, O. and Gurfil, P., "Long-Term Cluster Flight of Multiple Satellites Using Differential Drag," *Journal of Guidance, Control, and Dynamics*, Vol. 36, No. 6, 2013, pp. 1731–1740.